Article

Not peer-reviewed version

Catalytic Oxidation of Acetone over MnOx-SiO2 Catalysts: An Effective Approach to Valorize Rice Husk Waste

Mauricio Cardoso , Patrice Portugau , Carolina De los Santos , Ricardo Faccio , Hilario Vidal , José Manuel Gatica , María Pilar Yeste , Jorge Castiglioni , Martín Torres Brunengo *

Posted Date: 15 November 2024

doi: 10.20944/preprints202411.1197.v1

Keywords: rice husk silica; biomass waste; VOC; manganese oxides; catalyst; air pollution

 doi:10.20944/preprints202411.1197.v1

Article

Catalytic Oxidation of Acetone Over MnO_x-SiO_2 Catalysts: An Effective Approach to Valorize Rice Husk Waste

Mauricio Cardoso [1], Patrice Portugau [1], Carolina De Los Santos [1], Ricardo Faccio [2], Hilario Vidal [3], Jose Manuel Gatica [3], María del Pilar Yesté [3], Jorge Castiglioni [1] and Martín Torres [1,*]

[1] Área Fisicoquímica, Facultad de Química, Universidad de la República. Gral. Flores 2124. Montevideo, Uruguay; mcardoso@fq.edu.uy (M.C.); portugau@fq.edu.uy (P.P.); cdlsantos@fq.edu.uy (C.D.L.S.); jcastig@fq.edu.uy (J.C.)

[2] Área Física, Facultad de Química, Universidad de la República. Gral. Flores 2124. Montevideo, Uruguay; rfaccio@fq.edu.uy

[3] Departamento C.M. I.M. y Química Inorgánica, Universidad de Cádiz, Puerto Real 11510, Spain; hilario.vidal@uca.es (H.V.); josemanuel.gatica@uca.es (J.M.G.); pili.yeste@uca.es (M.d.P.Y.)

* Correspondence: mtobru@fq.edu.uy

Abstract: Rice husk, a byproduct of rice production, presents significant environmental challenges due to its disposal, while the emission of volatile organic compounds into the atmosphere poses additional concerns. This study addresses these issues by exploring the potential of texturally modified SiO_2 derived from Uruguayan rice husk as a catalytic support for manganese oxides in volatile organic compounds combustion. SiO_2 was synthesised from rice husk ash using a sustainable, acid-free pretreatment method, yielding a notably high silica purity of 96.5%—a level comparable to or exceeding those reported in previous studies, and underscoring the high silica quality inherent in Uruguayan rice husk. The catalytic performance of the catalysts was evaluated using acetone as a model of volatile organic compound, achieving up to 90% conversion with 30 wt.% manganese oxide at 300 °C, primarily yielding CO_2. Furthermore, a 24-hour stability test indicated consistent conversion, maintaining around 95.6 ± 2.5%. These findings suggest that Uruguayan rice husk-derived SiO_2, with its high purity and sustainability benefits, offers an effective solution for acetone removal when supporting an active phase such as manganese oxides, addressing both rice husk disposal and volatile organic compounds emissions.

Keywords: rice husk silica; biomass waste; VOC; manganese oxides; catalyst; air pollution

1. Introduction

The conversion of biomass waste globally to produce value-added materials is a current trend, which has been boosted by the United Nations Sustainable Development Goals. One of the main objectives is the modernization of infrastructure and the conversion of industries towards sustainability, through more efficient use of resources and the promotion of the adoption of clean and environmentally responsible technologies and industrial processes. This implies that all countries must take measures according to their respective capacities [1].

In this sense, Uruguay is renowned for being an agrarian country that extensively utilizes its soil for various crops, particularly rice. In 2022-2023 season, the estimated rice harvest reached 1,462,800 tons, as reported by the competent ministry of Uruguay [2]. This production volume places Uruguay among the top 10 rice producers [3]. The primary product of the rice crop is paddy rice, accounting for 80% of the total harvested mass [4], and the remaining 20% corresponds to rice husk (RH), which is predominantly used for energy production due to its high calorific value of 14.7 MJ kg^{-1} [5]. There are in Uruguay two energy production plants that utilize RH as a fuel source [6]. Despite its extensive

 doi:10.20944/preprints202411.1197.v1

use as energy source, a great portion of rice husk produced remain useless and it is deposited in several places including water courses, causing diverse environmental deterioration [4]. This fact rises concern to the Uruguayan academic community, who has been exploring multiple RH management and valorization, including energy storage and production of antioxidants, among others [7–9]. In the case of using RH to produce energy, the challenge implies the management of large quantities of ashes, which are composed by amorphous SiO_2 (90-95%) [4,10]. These produced ashes are not widely utilized, and they are finally deposited in the environment, causing soil acidification and alterations of its physicochemical properties [11]. The abundance of SiO_2 in the RH ash has been proposed for assessment as a new material with diverse applications [4].

The SiO_2 obtained from RH combustion at temperatures below 800 °C is mainly amorphous, requiring modification of its textural properties for being used in material science. These textural modifications are achieved via a reaction sequence that results in high specific surface areas [12]. Texturally modified SiO_2 derived from RH has multiple applications, including adsorption, supercapacitors, controlled release systems, catalysis, among others [4,10,13–15].

SiO_2 has been evaluated as catalyst support by incorporating active species. This utilization has been extensively reported in numerous papers encompassing a wide range of reactions, such as remediation of contaminants in water, Fischer-Tropsch reaction, hydrogenation reactions, and combustion of volatile organic compounds (VOCs). For this latter case, the active phase used was copper and palladium [16–19].

Currently, atmospheric pollution has become a significant concern for the scientific community. The emission of VOCs into the atmosphere because of industrial and anthropogenic activities has numerous environmental and human health impacts due to their toxicity and its contribution to the formation of ground-level ozone and photochemical smog [20,21]. Therefore, catalytic combustion appears to be a promising solution to prevent the emission of VOCs into the atmosphere [21]. In this regard, catalysts incorporating manganese as the active phase have exhibited a broad catalytic efficacy for the conversion of volatile organic compounds [22].

Manganese is one of the most abundant metals on earth crust, resulting in the availability of cost-effective manganese compounds. This transition metal possesses five unpaired electrons in the *d* level, enabling it to exhibit multiple oxidation states and constituting a wide range of stable oxides (MnO_x) [23]. Moreover, manganese is capable of transitioning between different oxidation states, for example MnO_2, Mn_2O_3, and Mn_3O_4 [24]. This capability can explain its excellent performance for oxidizing VOCs. Despite its catalytic combustion capabilities, processing gas streams containing VOCs needs large quantities of MnO_x due to its low specific surface area (<5 $m^2\ g^{-1}$). Consequently, supporting MnO_x onto a mesoporous solid allows enhancing dispersion and increasing atomic efficiency, being it an alternative method to increase specific surface area and therefore to improve catalytic performance [25].

Our research group has assessed the purity of the RH ash in terms of SiO_2, obtained from Uruguayan RH, and the results showed that it is higher than 95% without requiring further purification steps. These results establish our RH as a high-purity silica source, distinguishing it from other studies in the field that require acid treatments to achieve similar purity [12,26]. Based on the aforementioned information, and considering that, to the best of authors' knowledge, this is the first time that RH ash is being evaluated from this perspective, the objective of this study is to obtain a new type of catalyst, characterize the texturally modified SiO_2 derived from Uruguayan rice husk ashes and assess its potential as a catalytic support for MnO_x in the catalytic combustion of a VOC, such as acetone. This represents a new application for the use of rice husk waste in the field of catalysis [27]. Furthermore, this study provides insights into a new method for valorizing rice husk ash, laying the groundwork for potential future solutions to two current environmental challenges.

 doi:10.20944/preprints202411.1197.v1

2. Materials and Methods

2.1. Synthesis of SiO_2

Rice *Olimar* variety was used as RH source, supplied by the Sociedad Anónima de Molinos Arroceros Nacionales (SAMAN). A pretreatment of RH was realized: a considerable amount of RH was ground, then sifted to collect a 50 g with a particle size between 0.60-0.80 mm. The sieved sample was washed with distilled water to remove soil and other soluble impurities before drying for 24 h at 105 °C. The synthesis of SiO_2 from RH was carried out through the technique described by [12] with a few modifications. The RH pretreated was directly calcined at 600 °C for 2 h to obtain its ashes in a muffle furnace, obtaining approximately 10 g of ashes. After the calcination step, the obtained RH ash was dissolved in NaOH (1 g of RH ash: 10 mL of NaOH 4 M) with continuous magnetic stirring and kept at 80 °C for 4 h, following scheme 1.

$$SiO_2(s) + 2NaOH\ (aq) \xrightarrow{\Delta} Na_2SiO_3\ (aq) + H_2O\ (l) \quad (1)$$

This solution was then cooled to room temperature and filtered. After measuring the pH value, the solution was stored in a propylene flask. Then, the solution was treated with the stoichiometric volume of HCl 5 M in one addition to reach pH of 9. When the target pH was achieved, this process causes the gelation of silicic acid that forms in the solution, as shown by scheme 2.

$$Na_2SiO_3\ (aq) + 2HCl\ (aq) \longrightarrow 2NaCl\ (aq) + H_2SiO_3\ (s) \quad (2)$$

This gel was washed several times with magnetic stirring to split it and ensure mass exchange during the washes until neutral pH and conductivity below 50 µS/cm. Subsequently, it was dried in an oven at 105 °C overnight. Finally, the solid obtained was calcined for 2 h at 600 °C in an air atmosphere to obtain SiO_2, according to scheme 3. The solid obtained was named "RHS".

2.2. Synthesis of Catalysts

$$H_2SiO_3\ (s) \xrightarrow{\Delta} SiO_2\ (s) + H_2O \quad (3)$$

Catalysts were synthesized through impregnation until incipient moisture method [24,28], using manganese acetate tetra-hydrate ($Mn(Ac)_2$) supplied by Sigma Aldrich (Purity > 99%) as MnO_x precursor. An appropriate amount of $Mn(Ac)_2$ was dissolved in distilled water in order to obtain a saturated solution. Then, an adequate amount of RHS was impregnated with this solution. Subsequently, the resulting impregnated solid was dried in an oven at 105 °C for 24 h, then it was calcined in a furnace using the following temperature program: from room temperature to 550 °C at a heating rate of 5 °C/min, then the sample was dwell for 4 h. This procedure is in accordance with the thermal analysis results (see below). Catalysts were named as MnXRHS, where X is the weight amount of manganese loaded onto RHS (10, 30 and 40%). Bulk manganese oxide, referred to as MnO_x, was synthesized using the same organic salt and temperature program.

2.3. Characterization Studies

2.3.1. X-Ray Diffraction (XRD) and Rietveld Analysis

X-Ray Powder diffraction (Rigaku Miniflex 600-C X-ray diffractometer) was performed in θ–θ geometry operating with CuKα X-Ray radiation source (sealed tube operating at 40 kV/30 mA) and a curved Ge crystal beam monochromator with a focal distance of 285 mm. Data were collected in the 2θ range of (2.00–70.00)°, and a 2θ step of 0.02°, with a counting of 2 s/step. Full pattern profile fitting through Rietveld refinement surface [29] was performed using Smart Lab Studio II from Rigaku.

 doi:10.20944/preprints202411.1197.v1

2.3.2. Thermogravimetric Analysis

Thermogravimetric analysis (TGA) was carried out in a Shimadzu TGA-50 equipment, using in each case 10 mg of sample under air stream (50 mL/min). In all cases, a platinum pan was used. For the TGA of rice husk, a heating program from room temperature to 900°C with a heating rate of 10 °C/min. In the case of the MnO_x precursor, the temperature program used was from room temperature to 550°C at 5°C/min, and it was then held at that temperature for 4 hours.

2.3.3. Microwave-Induced Plasma Atomic Emission Spectrometry

The purity of the RHS ash was measured using microwave-induced plasma atomic emission spectrometry with an Agilent 4210 MIP OES system. For this analysis, 250 mg of sample was dissolved in 15 mL of 0.5 mol/L KOH, sonicated for 20 minutes, and subsequently treated in a water bath at 80 °C for 3 hours.

2.3.4. Textural Characterization

Textural characterization was performed by means of N_2 physisorption at 77 K with a Micromeritics ASAP2020. For this analysis, all the samples were pre-evacuated at 200 °C for 2 h. The specific surface area was calculated by the BET method. Total pore volume (V_{total}) was estimated from the amount of nitrogen adsorbed at relative pressures of 0.99.

2.3.5. Fourier Transformed Infrared Spectroscopy

FTIR were obtained with a FT-IR, Shimadzu QATR-S IRSpirit in a range of 4000–400 cm^{-1}, measurement mode %Transmittance, Attenuated Total Reflection (ATR) mode Single Reflection ATR Accessory (QATR-S).

2.3.6. Scanning Electron Microscopy (SEM) and Energy Dispersion Spectroscopy (EDS)

SEM analysis was performed on uncoated samples. The samples were placed into an aluminium sample holder using carbon tape and then introduced to a JEOL JS M-5900LV Scanning Electron Microscope under a constant voltage supply of 25 kV, equipped with an Energy Dispersive Spectrometer probe under 20 kV of voltage supply (NORAN system 7 instruments EDS limited advantage).

2.3.7. Temperature Programmed Reduction Mass Spectrometry (H_2-TPR)

H_2-TPR experiments were performed on an Autochem Micromeritics apparatus with a thermal conductivity detector (TCD). Prior to the measurement, all samples were treated in Ar at 500°C for 1 h (60 mL/min) and then cooled to 25°C. Then, during TPR in H_2, a current of 5% H_2/Ar (60 mL/min) was used, and the samples were heated to 900°C (ramp 10°C/min) for 1 h.

2.4. Catalytic Evaluation

To evaluate the performance of the catalysts for the oxidation of acetone, samples of 500 mg were placed into a quartz reactor with U shape. In the assays, oxygen was bubbled in liquid acetone at (0 ± 1) °C using a flow of 6.5 $cm^3\ min^{-1}$ and then mixed with the argon flow (120 $cm^3\ min^{-1}$). The GHSV value was ~15000 $cm^3\ h^{-1}\ g_{cat}^{-1}$. For each assay, the temperature was increased from 150 °C to 500 °C, collecting samples from the inlet and outlet every 50 °C for monitoring gas composition. Gases were analyzed using a Shimadzu Gas Chromatograph GC-2014 with a Hayesep® column. The stability test of the best catalyst was performed under the same flow conditions for 24 h. However, the temperatures for carrying out this test were chosen based on the *light-off* curves obtained.

 doi:10.20944/preprints202411.1197.v1

3. Results and Discussion

3.1. Characterization Results

In the thermogravimetric analysis depicted in Figure 1.a, RH exhibits three mass loss steps: the first due to moisture in the raw sample, while the subsequent two result from organic matter decomposition, consistent with the literature [8]. Above 500 °C, the mass stabilizes at 20%, attributed to ash content. Figure 1.b presents thermal analysis for RHS and $Mn(Ac)_2$, noting that RHS exhibits no weight loss above 105 °C, with mass loss only from humidity below 100 °C. The decomposition of $Mn(Ac)_2$ to form MnO_x aligns with previous studies [24]. Consequently, the calcination temperature for the catalysts was set at 550 °C.

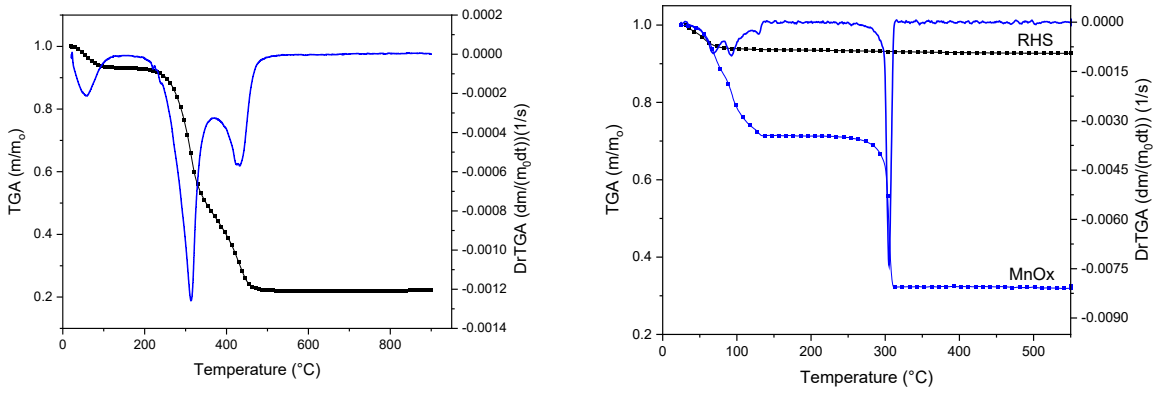

(a) (b)

Figure 1. Thermogravimetric analysis results obtained for (a) RH and (b) RHS and manganese acetate, which is the precursor of bulk MnO_x.

The SiO_2 content determined using the ICP in RHS was 96.5 wt. %, confirming the high purity of silica in our rice husk sample. Additionally, the sodium content, quantified as Na_2O, was found to be 2.47 wt. %. Compared to previous studies that employed acid-based extraction methods [12,26], this approach presents a more sustainable alternative due to its lower energy requirements. The acid-free extraction method not only enhances sustainability by minimizing chemical usage and energy consumption, but also reinforces the purity of our RHS, highlighting its potential as a cost-effective and environmentally responsible source of high-purity silica for various applications.

Figure 2 shows RHS diffractogram which presents the typical broad dispersion of amorphous SiO_2 in the $2\boldsymbol{\theta}$ range around 20-30° [30]. On the other hand, bulk MnO_x diffractogram presents a diffraction pattern which fits with the crystalline structure of $\boldsymbol{\alpha}-Mn_2O_3$ (Bixbyite, cubic crystalline system, space group $\boldsymbol{Ia\bar{3}}$) [24] as shown in Figure S.1. According to a full pattern profile fitting and to the Rietveld refinement [29,31], the refined crystalline size domain value corresponds to D = 26.8 (4) nm, in a nanosized domain. The synthesized catalysts (Mn10RHS, Mn30RHS, and Mn40RHS) present similar crystalline structure and their broad reflections are related to the presence of amorphous SiO_2, which indicates the structural stability of the support. In the case of supported catalysts, the diffraction pattern fits with the crystalline structure of majority Mn_3O_4 (Hausmannite, tetragonal crystalline system, space group $\boldsymbol{I4_1/amd}$) and minority $\boldsymbol{\beta}$-MnO_2 (Pyrolusite, tetragonal crystalline system, space group $\boldsymbol{P4_2/mnm}$) [32] as shown in Figure S.2. The corresponding Bragg reflections present important full widths at half maximum (FWHM), indicating a possible confinement effect according to Scherrer [33]. Due to this broadening and the proximity in the Bragg reflections between Mn_3O_4 and $\boldsymbol{\beta}$-MnO_2, the samples could confirm both phases. We proceed with an internal standard procedure using yttrium oxide (cubic crystalline system, space group $\boldsymbol{Ia\bar{3}}$) as a reference pattern to determine relative weight fractions of the crystalline and amorphous components. For Mn40RHS we obtained a crystalline size domain value close to D=30.9(5) nm and relative weight fraction on crystalline basis of 17.44(2) %, 0.04(2) %, and 82.5(2) % for Mn_3O_4, $\boldsymbol{\beta}$-MnO_2 and amorphous phase, respectively. In the case of Mn30RHS, we refined a crystalline size domain of

 doi:10.20944/preprints202411.1197.v1

D=18.4(5) nm with a relative weight fraction of 14.4(4) %, 1.1(4) %, and 84.5 % for an amorphous phase, respectively. Finally, in the case of Mn10RHS, we obtained a D=10(1) nm for Mn_3O_4 exclusively with a relative weight fraction of 5.7(4) %, accompanied by an amorphous fraction of 94.3%. The difference between the crystalline structure of bulk MnO_x and the crystalline structure of supported catalysts reveals the interaction of SiO_2 surface during the formation of MnO_x. Additionally, there are differences in the evolution of the crystalline unit cell parameters, for the majority phase Mn_3O_4, with a= 5.7646(3)Å, a= 5.7737(16)Å and a= 5.784(9)Å, for Mn40RHS, Mn30RHS and Mn10RHS, respectively. As mentioned above, the reducibility of Mn_2O_3 is different to that of Mn_3O_4, thus, its catalytic performance is expected to be also different.

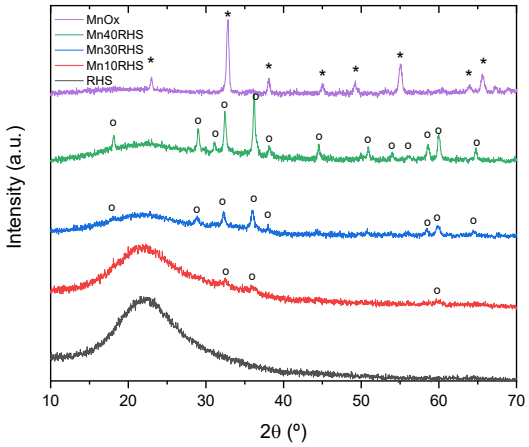

Figure 2. X-Ray powder diffraction patterns for bulk MnO_x, Mn40RHS, Mn30RHS, Mn10RHS and RHS. Peaks associated with Mn_2O_3 (*) and peaks associated with Mn_3O_4 (°).

The N_2 physisorption isotherm presented in Figure 3.a, along with the corresponding pore size distribution (PSD) in Figure 3.b, illustrates the characteristics of all catalysts. According to IUPAC classification [34], the isotherms are primarily type II with H3 hysteresis. The PSD profiles for all catalysts and the RHS support are similar; however, the pores around 1 nm decrease as the manganese phase increases, resulting in reduced microporosity of the samples.

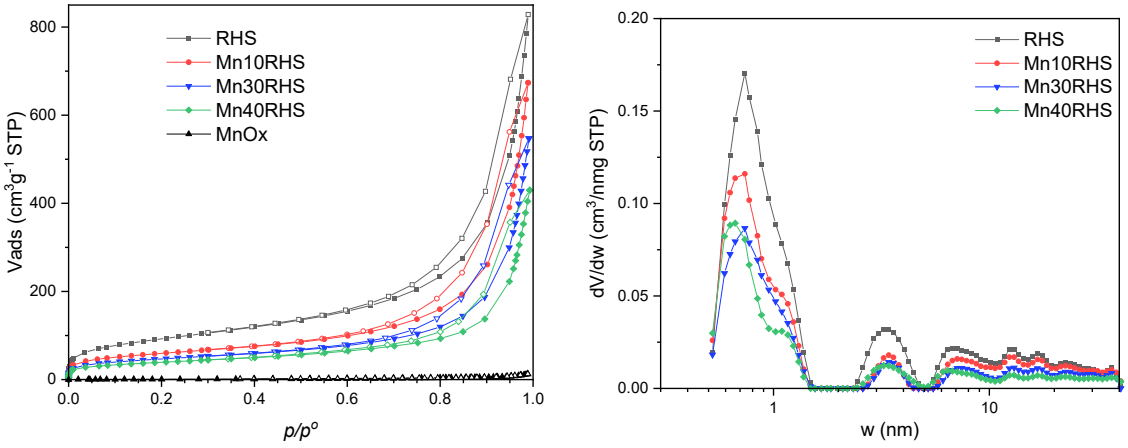

Figure 3. Nitrogen adsorption-desorption isotherms of the catalyst samples (a) and pore size distribution curves obtained through NLDFT (b).

Table 1 lists the textural parameters and specific surface area (S_{BET}) for the catalysts, with RHS exhibiting a S_{BET} of 333 m^2/g, indicating a favorable surface area compared to other silica supports derived from RH ash [12]. For supported catalysts, S_{BET} decreases with increasing MnOx loading, a trend also observed in total pore volume (V_{Tp}). This behavior likely results from the reduction of

 doi:10.20944/preprints202411.1197.v1

mesoporous volume (V_{mp}) and micropore volume ($V_{\mu p}$) due to catalyst deposition and subsequent pore coverage.

Table 1. Textural parameters for synthesized catalysts.

Sample	S_{BET}	V_{tp}	V_{mp}	$V_{\mu p}$
	m^2/g		cm^3/g	
RHS	333	0.790	0.707	0.083
Mn10RHS	215	0.609	0.551	0.058
Mn30RHS	169	0.470	0.425	0.045
Mn40RHS	141	0.348	0.308	0.040
MnOx	2	0.013	0.013	0.000

The FT-IR analysis of the synthesized catalysts and RHS, as shown in Figure 4, reveals that RHS displays three main bands at 453 cm^{-1} and 1070 cm^{-1}, corresponding to Si-O-Si bonds, and at 802 cm^{-1}, related to silanol groups (Si-OH) on the surface. These silanol groups may interact with the carbonyl groups of acetone molecules, the VOC model used in this work, potentially impacting catalytic performance [21]. Bulk MnOx exhibits broad bands between 350-600 cm^{-1}, with peak absorption around 480 cm^{-1} [32]. However, the specific phase of Mn_2O_3 (α or γ) cannot be determined from this analysis due to the similarity of FT-IR patterns reported in the literature [32]. Despite this limitation, the results align with the XRD findings. For the Mn40RHS and Mn30RHS catalysts, two characteristic peaks of Mn_3O_4 are identified at 475 cm^{-1} and 594 cm^{-1} [32]. In contrast, the FT-IR spectrum of Mn10RHS is similar to that of RHS.

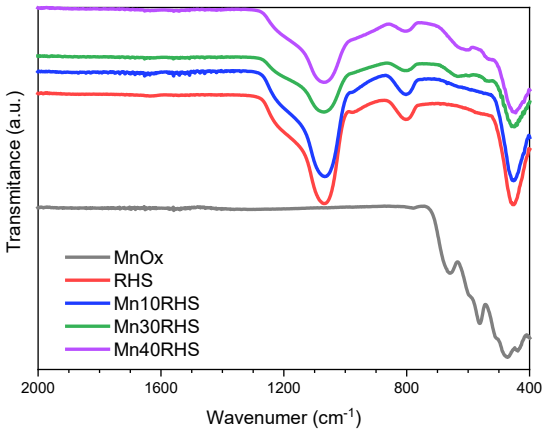

Figure 4. FT-IR spectra for the catalysts.

The results of SEM analysis and EDS mapping are presented in Figure 5. The SEM image of MnOx (5.i and 5.j) reveals particles agglomeration, in contrast to the catalysts Mn10RHS (5.c and 5.d), Mn30RHS (5.e and 5.f), and Mn40RHS (5.g and 5.h). EDS mapping was conducted to evaluate the distribution of manganese oxide on the RHS surface, showing no agglomeration zones for the manganese phase, which indicates a homogeneous distribution.

 doi:10.20944/preprints202411.1197.v1

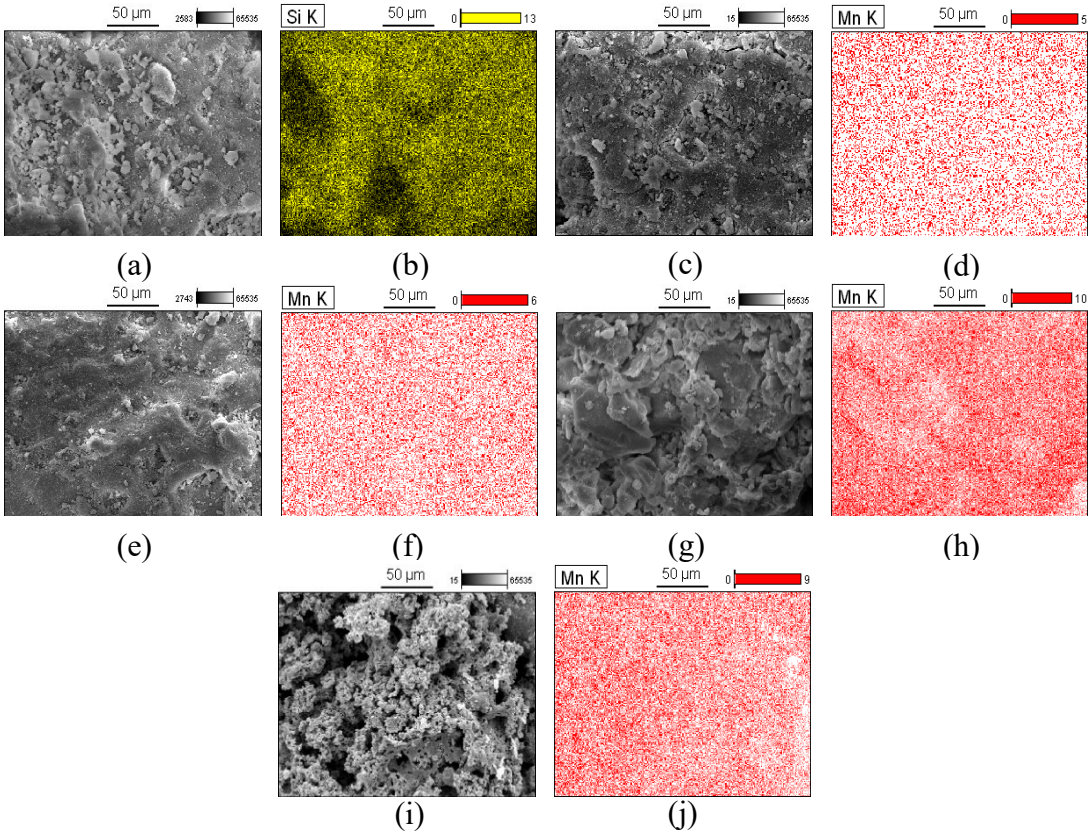

Figure 5. SEM micrographs and EDS mapping obtained for a) and b) RHS; c) and d) Mn10RHS; e) and f) Mn30RHS; g) and h) Mn40RHS; i) and j) MnO_x. All figures were taken using a magnification of x800.

The H_2-TPR results depicted in Figure 6 illustrate the reduction behavior of the catalyst components, including the support and the catalytic phase. For MnO_x, a two-step reduction is observed, with peaks at 450 °C and 510 °C. In contrast, the reduction of Mn40RHS occurs in a single step, peaking at 445 °C, while RHS shows no reduction. The total H_2 consumed (O/Mn) is 0.46 for MnO_x, indicating that the starting oxide was Mn_2O_3, which was subsequently reduced to Mn_3O_4 and MnO. The Mn40RHS catalyst shows an H_2 consumption corresponding to a 0.30 O/Mn ratio, suggesting that the starting oxide is Mn_3O_4, consistent with its single-peak reduction profile. This increase in the oxidation state of manganese with its content aligns with the literature [35]. Additionally, the more intense low-temperature reduction peak for Mn40RHS can be attributed to a higher dispersion of the manganese phase on the support.

 doi:10.20944/preprints202411.1197.v1

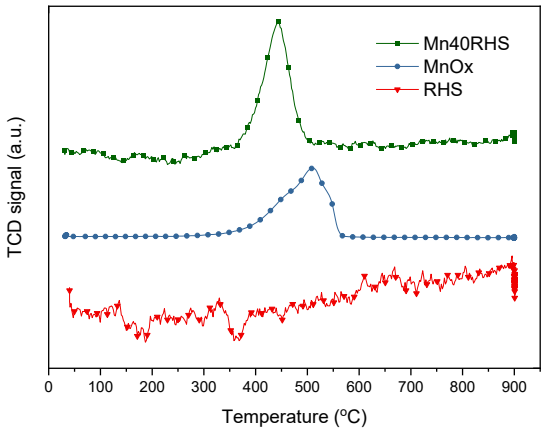

Figure 6. H_2-TPR for bulk MnO_x, Mn40RHS and RHS.

3.2. Activity Testing

The *light-off* curves for the catalysts using acetone as a VOC model are presented in Figure 7. All catalysts and the support demonstrate activity in the catalytic conversion of acetone. For the catalysts containing MnO_x, acetone oxidation is known to occur via a Mars-Van Krevelen mechanism [36,37].

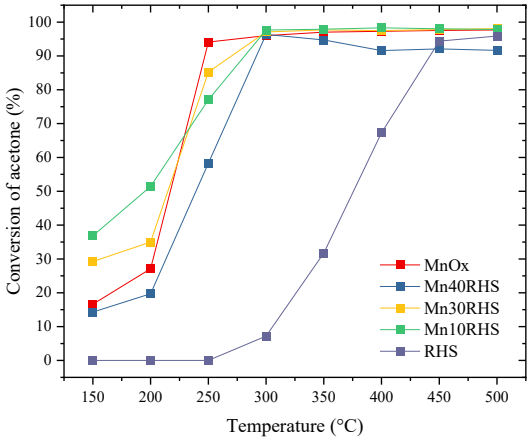

Figure 7. *Light-off* curves obtained for acetone oxidation.

For RHS, catalytic activity begins above 250 °C, reaching conversion values of up to 90% at 450 °C. This conversion can be partly attributed to the presence of silanol groups on the RHS surface [21]. Bulk MnO_x achieves over 90% acetone conversion at 250 °C, while the supported catalysts—Mn10RHS, Mn30RHS, and Mn40RHS—match this performance at 300 °C. Although RHS shows activity above 250 °C, it does not reach 10% acetone conversion at 300 °C, indicating its contribution to acetone oxidation is smaller but not negligible, supporting its role as a catalytic support.

Moreover, the light-off curves demonstrate the effectiveness of supporting the active phase on RHS at contents below 50%. Under the specified temperature conditions, Mn30RHS and Mn40RHS achieve complete conversion to CO_2. This behavior is summarized in Table 2, which presents the ratio (R) between experimentally quantified CO_2 and CO_2 calculated from the total combustion of acetone, based on experimental conversion at various temperatures. The ratios were evaluated at T_{85} and T_{95}, the temperatures at which 85% and 95% acetone conversion are reached, respectively, along with the temperature at which a ratio of 1 indicates total conversion to CO_2.

 doi:10.20944/preprints202411.1197.v1

Table 2. Values of T_{85}, T_{95}, R, and temperature at which R=1, obtained from light-off curves and calculated from GC Data.

Parameter	Mn10RHS	Mn30RHS	Mn40RHS
T_{85} $(°C)$	269	245	285
$R_{T_{85}}$	0.51	0.86	0.85
$T_{95}(°C)$	294	291	298
$R_{T_{95}}$	0.72	0.92	0.94
$T_{R=1}$ $(°C)$	-	300	300

While the Mn10RHS catalyst achieved conversions above 90%, it did not attain complete conversion of acetone to CO_2. In contrast, the Mn30RHS and Mn40RHS catalysts demonstrated significantly better performance, reaching an R value of 1 at 300 °C. This improvement is likely due to better surface coverage of the support in Mn30RHS and Mn40RHS, attributed to higher loading compared to Mn10RHS, despite all catalysts displaying similar phases according to XRD.

Among the Mn30RHS and Mn40RHS catalysts, Mn30RHS exhibited the lowest T_{85} and T_{95} temperatures (see Table 2), indicating superior performance in acetone oxidation. This enhanced activity may stem from its higher surface area, larger pore and mesopore volumes, and improved distribution, as supported by N_2 physisorption and SEM results. Thus, Mn30RHS is more effective for acetone conversion, allowing for a smaller amount of active phase when using SiO_2 derived from RH.

The positive results for acetone conversion align with prior research [38], which indicates that the presence of a carbonyl group in acetone enhances its catalytic oxidation [21]. Moreover, [39] reported that a pillared montmorillonite with 10% manganese oxide required 342 °C to achieve 90% conversion, suggesting that our catalyst outperforms previously reported catalysts in acetone oxidation.

With Mn30RHS identified as the best supported catalyst for acetone, achieving conversions above 90%, its catalytic stability was evaluated over 24 hours under the same flow conditions used for catalytic testing, but at 300 °C, where an R value of 1 is assured. Results are presented in Figure 8.

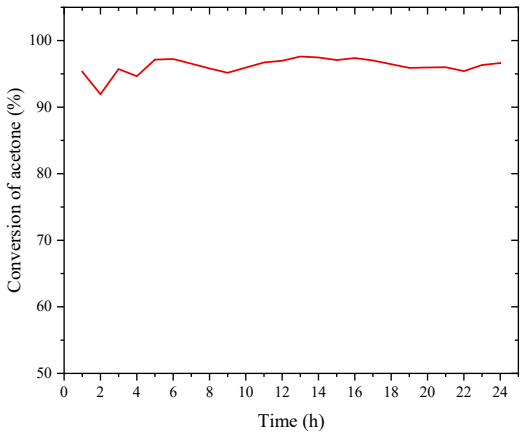

Figure 8. Stability test performed to Mn30RHS during 24 hours for acetone.

In this case, the stability tests yielded remarkable results, as no deactivation was observed, and the conversion remained virtually constant within the range of (95.6 ± 2.5) %. Additionally, the R ratio was closely monitored, and its value also remained steady within the range of (0.9 ± 0.1).

4. Conclusions

This work involved the preparation, characterization, and evaluation of catalysts with varying loads of MnOx supported on mesoporous SiO_2 derived from Uruguayan rice husk ashes. The silica

 doi:10.20944/preprints202411.1197.v1

from RH ash proved to be a promising catalytic support, achieving over 90% acetone conversion at 450 °C, with improved textural properties compared to previous results.

All catalysts demonstrated activity in acetone oxidation, with Mn30RHS and Mn40RHS showing notable conversion to CO_2. Among the catalysts examined, Mn30RHS yielded the best overall performance. Notably, comparable catalytic behavior to bulk MnOx was achieved at 300 °C, allowing for a reduced quantity of transition metal oxide when supported on RHS.

This study highlights that SiO_2 derived from Uruguayan rice husk ashes can effectively contribute to the development of mesoporous-MnOx catalysts for VOC removal, offering potential solutions for ash deposition and improving air quality.

Supplementary Materials: The following supporting information can be downloaded at the website of this paper posted on Preprints.org. Figure S1: Rietveld profile fitting for a) Mn40RHS, b) Mn30RHS and c) Mn10RHS samples including yttria.; Table S1: Summary of main statistics of the Rietveld refinement for Mn40RHS, Mn30RHS and Mn10RHS.

Author Contributions: Mauricio Cardoso: Validation, Formal analysis, Investigation, Software, Writing - Original Draft, Visualization. Patrice Portugau: Validation, Formal analysis, Investigation, Software, Writing - Original Draft, Visualization, Writing - Review & Editing. Carolina de los Santos: Validation, Formal analysis, Investigation, Writing - Original Draft, Visualization, Writing - Review & Editing. Ricardo Faccio: Validation, Formal analysis, Investigation, Software, Writing - Original Draft, Visualization, Writing - Review & Editing. Hilario Vidal: Writing - Original Draft, Visualization, Writing - Review & Editing. José Manuel Gatica: Writing - Original Draft, Visualization, Writing - Review & Editing. Maria del Pilar Yesté: Validation, Formal analysis, Investigation, Writing - Original Draft, Visualization, Writing - Review & Editing.Jorge Castiglioni: Conceptualization, Methodology, Writing - Review & Editing, Supervision, Project administration, Funding acquisition. Martin Torres Brunengo: Validation, Formal analysis, Resources, Investigation, Writing - Original Draft, Visualization, Conceptualization, Methodology, Software, Writing - Review & Editing, Supervision, Project administration, Funding acquisition

Funding: This research was funded by Comisión Sectorial de Investigación Científica, grant number I+D 2115-347.

Data Availability Statement: The original contributions presented in the study are included in the article, further inquiries can be directed to the corresponding authors.

Acknowledgments: Authors would thank Comisión Sectorial de Investigación Científica, project CSIC I+D 2115-347 for the funding gave to carry out the research and to SAMAN for the rice husk samples. Authors would also acknowledge PEDECIBA for the financial support. The authors also thank Prof. Dr. Mariela Piston and MSc. Marcelo Belluzzi for their assistance with the ICP analysis.

Conflicts of Interest: The authors declare no conflicts of any commercial or associative interest in connection with the work submitted.

References

[1] United Nations. United Nations Sustainable Development Goals https://www.un.org/sustainabledevelopment/infrastructure-industrialization/ (accessed May 1, 2024).
[2] Salgado, L. Arroz: situación y perspectivas. https://www.gub.uy/ministerio-ganaderia-agricultura-pesca/comunicacion/publicaciones/anuario-opypa-2022/analisis-sectorial-cadenas-productivas/arroz (accessed Mar 25, 2024).
[3] Uruguay XXI. Sector agrícola en Uruguay https://www.uruguayxxi.gub.uy/uploads/informacion/20c2018b1a2e68514020b55bcd11b62c6874640e.pdf (accessed Mar 25, 2024).
[4] Gebretatios, A. G.; Kadiri Kanakka Pillantakath, A. R.; Witoon, T.; Lim, J.-W.; Banat, F.; Cheng, C. K. Rice Husk Waste into Various Template-Engineered Mesoporous Silica Materials for Different Applications: A Comprehensive Review on Recent Developments. *Chemosphere*, **2023**, *310*, 136843. https://doi.org/10.1016/j.chemosphere.2022.136843.
[5] Torres, M.; Portugau, P.; Castiglioni, J.; Yermán, L.; Cuña, A. Evaluation of the Potential Utilization of Conventional and Unconventional Biomass Wastes Resources for Energy Production. *Renewable Energy and Power Quality Journal*, **2019**, 511–515. https://doi.org/10.24084/repqj17.360.

[6] MGAP. Plantas de operación https://www.gub.uy/ministerio-industria-energia-mineria/publicaciones/plantas-operacion (accessed Mar 25, 2024).

[7] Xavier, L.; Rocha, M.; Pisani, J.; Zecchi, B. Aqueous Two-Phase Systems Based on Cholinium Ionic Liquids for the Recovery of Ferulic and p-Coumaric Acids from Rice Husk Hydrolysate. *Applied Food Research*, **2024**, *4* (1), 100381. https://doi.org/10.1016/j.afres.2023.100381.

[8] Leal da Silva, E.; Torres, M.; Portugau, P.; Cuña, A. High Surface Activated Carbon Obtained from Uruguayan Rice Husk Wastes for Supercapacitor Electrode Applications: Correlation between Physicochemical and Electrochemical Properties. *J Energy Storage*, **2021**, *44*, 103494. https://doi.org/10.1016/j.est.2021.103494.

[9] Torres, M.; Portugau, P.; Castiglioni, J.; Cuña, A.; Yermán, L. Co-Combustion Behaviours of a Low Calorific Uruguayan Oil Shale with Biomass Wastes. *Fuel*, **2020**, *266*, 117118. https://doi.org/10.1016/j.fuel.2020.117118.

[10] Adam, F.; Appaturi, J. N.; Iqbal, A. The Utilization of Rice Husk Silica as a Catalyst: Review and Recent Progress. *Catal Today*, **2012**, *190* (1), 2–14. https://doi.org/10.1016/j.cattod.2012.04.056.

[11] Moraes, C. A.; Fernandes, I. J.; Calheiro, D.; Kieling, A. G.; Brehm, F. A.; Rigon, M. R.; Berwanger Filho, J. A.; Schneider, I. A.; Osorio, E. Review of the Rice Production Cycle: By-Products and the Main Applications Focusing on Rice Husk Combustion and Ash Recycling. *Waste Management & Research: The Journal for a Sustainable Circular Economy*, **2014**, *32* (11), 1034–1048. https://doi.org/10.1177/0734242X14557379.

[12] Santana Costa, J. A.; Paranhos, C. M. Systematic Evaluation of Amorphous Silica Production from Rice Husk Ashes. *J Clean Prod*, **2018**, *192*, 688–697. https://doi.org/10.1016/j.jclepro.2018.05.028.

[13] Andrade, J. de L.; Moreira, C. A.; Oliveira, A. G.; de Freitas, C. F.; Montanha, M. C.; Hechenleitner, A. A. W.; Pineda, E. A. G.; de Oliveira, D. M. F. Rice Husk-Derived Mesoporous Silica as a Promising Platform for Chemotherapeutic Drug Delivery. *Waste Biomass Valorization*, **2022**, *13* (1), 241–254. https://doi.org/10.1007/s12649-021-01520-z.

[14] Araichimani, P.; Prabu, K. M.; Kumar, G. S.; Karunakaran, G.; Surendhiran, S.; Shkir, Mohd.; AlFaify, S. Rice Husk-Derived Mesoporous Silica Nanostructure for Supercapacitors Application: A Possible Approach for Recycling Bio-Waste into a Value-Added Product. *Silicon*, **2022**, *14* (15), 10129–10135. https://doi.org/10.1007/s12633-022-01699-3.

[15] Sinyoung, S.; Kunchariyakun, K.; Asavapisit, S.; MacKenzie, K. J. D. Synthesis of Belite Cement from Nano-Silica Extracted from Two Rice Husk Ashes. *J Environ Manage*, **2017**, *190*, 53–60. https://doi.org/10.1016/j.jenvman.2016.12.016.

[16] Ernst, B.; Libs, S.; Chaumette, P.; Kiennemann, A. Preparation and Characterization of Fischer–Tropsch Active Co/SiO2 Catalysts. *Appl Catal A Gen*, **1999**, *186* (1–2), 145–168. https://doi.org/10.1016/S0926-860X(99)00170-2.

[17] Lambert, S.; Cellier, C.; Gaigneaux, E. M.; Pirard, J.-P.; Heinrichs, B. Ag/SiO2, Cu/SiO2 and Pd/SiO2 Cogelled Xerogel Catalysts for Benzene Combustion: Relationships between Operating Synthesis Variables and Catalytic Activity. *Catal Commun*, **2007**, *8* (8), 1244–1248. https://doi.org/10.1016/j.catcom.2006.11.018.

[18] Sitthisa, S.; Sooknoi, T.; Ma, Y.; Balbuena, P. B.; Resasco, D. E. Kinetics and Mechanism of Hydrogenation of Furfural on Cu/SiO2 Catalysts. *J Catal*, **2011**, *277* (1), 1–13. https://doi.org/10.1016/j.jcat.2010.10.005.

[19] Peralta, Y. M.; Molina, R.; Moreno, S. Chemical and Structural Properties of Silica Obtained from Rice Husk and Its Potential as a Catalytic Support. *J Environ Chem Eng*, **2024**, *12* (2), 112370. https://doi.org/10.1016/j.jece.2024.112370.

[20] Bratan, V.; Vasile, A.; Chesler, P.; Hornoiu, C. Insights into the Redox and Structural Properties of CoOx and MnOx: Fundamental Factors Affecting the Catalytic Performance in the Oxidation Process of VOCs. *Catalysts*, **2022**, *12* (10), 1134. https://doi.org/10.3390/catal12101134.

[21] Guo, Y.; Wen, M.; Li, G.; An, T. Recent Advances in VOC Elimination by Catalytic Oxidation Technology onto Various Nanoparticles Catalysts: A Critical Review. *Appl Catal B*, **2021**, *281*, 119447. https://doi.org/10.1016/j.apcatb.2020.119447.

[22] Zhu, J.; Cheng, Y.; Wang, Z.; Zhang, J.; Yue, Y.; Qian, G. Low-Energy Production of a Monolithic Catalyst with MnCu-Synergetic Enhancement for Catalytic Oxidation of Volatile Organic Compounds. *J Environ Manage*, **2023**, *336*, 117688. https://doi.org/10.1016/j.jenvman.2023.117688.

[23] Ghosh, S. K. Diversity in the Family of Manganese Oxides at the Nanoscale: From Fundamentals to Applications. *ACS Omega*, **2020**, *5* (40), 25493–25504. https://doi.org/10.1021/acsomega.0c03455.

[24] Torres, M.; de los Santos, C.; Portugau, P.; Yeste, M. D. P.; Castiglioni, J. Utilization of a PILC-Al Obtained from Uruguayan Clay as Support of Mesoporous MnOx-Catalysts on the Combustion of Toluene. *Appl Clay Sci*, **2021**, *201*, 105935. https://doi.org/10.1016/j.clay.2020.105935.

[25] Gatica, J. M.; Castiglioni, J.; de los Santos, C.; Yeste, M. del P.; Cigredo, G.; Torres, M.; Vidal, H. Clay Honeycomb Monoliths as Support of Manganese Catalysts for VOCs Oxidation. *International Journal of Chemical and Enviromental Engineering*, **2015**, *6* (4).

[26] Steven, S.; Restiawaty, E.; Pasymi, P.; Bindar, Y. An Appropriate Acid Leaching Sequence in Rice Husk Ash Extraction to Enhance the Produced Green Silica Quality for Sustainable Industrial Silica Gel Purpose. *J Taiwan Inst Chem Eng*, **2021**, *122*, 51–57. https://doi.org/10.1016/j.jtice.2021.04.053.

[27] Nzereogu, P. U.; Omah, A. D.; Ezema, F. I.; Iwuoha, E. I.; Nwanya, A. C. Silica Extraction from Rice Husk: Comprehensive Review and Applications. *Hybrid Advances*, **2023**, *4*, 100111. https://doi.org/10.1016/j.hybadv.2023.100111.

[28] Rashid, U.; Soltani, S.; Al-Resayes, S. I.; Nehdi, I. A. Metal Oxide Catalysts for Biodiesel Production. In *Metal Oxides in Energy Technologies*; Elsevier, 2018; pp 303–319. https://doi.org/10.1016/B978-0-12-811167-3.00011-0.

[29] Rietveld, H. M. A Profile Refinement Method for Nuclear and Magnetic Structures. *J Appl Crystallogr*, **1969**, *2* (2), 65–71. https://doi.org/10.1107/S0021889869006558.

[30] Mattos, B. D.; Rojas, O. J.; Magalhães, W. L. E. Biogenic SiO2 in Colloidal Dispersions via Ball Milling and Ultrasonication. *Powder Technol*, **2016**, *301*, 58–64. https://doi.org/10.1016/j.powtec.2016.05.052.

[31] Toby, B. H.; Von Dreele, R. B. GSAS-II : The Genesis of a Modern Open-Source All Purpose Crystallography Software Package. *J Appl Crystallogr*, **2013**, *46* (2), 544–549. https://doi.org/10.1107/S0021889813003531.

[32] Julien, C. M.; Massot, M.; Poinsignon, C. Lattice Vibrations of Manganese Oxides. *Spectrochim Acta A Mol Biomol Spectrosc*, **2004**, *60* (3), 689–700. https://doi.org/10.1016/S1386-1425(03)00279-8.

[33] Patterson, A. L. The Scherrer Formula for X-Ray Particle Size Determination. *Physical Review*, **1939**, *56* (10), 978–982. https://doi.org/10.1103/PhysRev.56.978.

[34] Thommes, M.; Kaneko, K.; Neimark, A. V.; Olivier, J. P.; Rodriguez-Reinoso, F.; Rouquerol, J.; Sing, K. S. W. Physisorption of Gases, with Special Reference to the Evaluation of Surface Area and Pore Size Distribution (IUPAC Technical Report). *Pure and Applied Chemistry*, **2015**, *87* (9–10), 1051–1069. https://doi.org/10.1515/pac-2014-1117.

[35] Fanelli, E.; Turco, M.; Russo, A.; Bagnasco, G.; Marchese, S.; Pernice, P.; Aronne, A. MnO x /ZrO2 Gel-Derived Materials for Hydrogen Peroxide Decomposition. *J Solgel Sci Technol*, **2011**, *60* (3), 426–436. https://doi.org/10.1007/s10971-011-2558-9.

[36] Kamal, M. S.; Razzak, S. A.; Hossain, M. M. Catalytic Oxidation of Volatile Organic Compounds (VOCs) – A Review. *Atmos Environ*, **2016**, *140*, 117–134. https://doi.org/10.1016/j.atmosenv.2016.05.031.

[37] Mars, P.; van Krevelen, D. W. Oxidations Carried out by Means of Vanadium Oxide Catalysts. *Chem Eng Sci*, **1954**, *3*, 41–59. https://doi.org/10.1016/S0009-2509(54)80005-4.

[38] Tichenor, B. A.; Palazzolo, M. A. Destruction of Volatile Organic Compounds via Catalytic Incineration. *Environmental Progress*, **1987**, *6* (3), 172–176. https://doi.org/10.1002/ep.670060328.

[39] Gandía, L. M.; Vicente, M. A.; Gil, A. Complete Oxidation of Acetone over Manganese Oxide Catalysts Supported on Alumina- and Zirconia-Pillared Clays. *Appl Catal B*, **2002**, *38* (4), 295–307. https://doi.org/10.1016/S0926-3373(02)00058-9.